**Advanced Steel Construction** – Vol. 22 No. 3 (2026) 315–322
**DOI:**10.18057/IJASC.2026.22.3.7


# STUDY ON SHEAR TEST AND CALCULATION METHOD OF CORROSION COLD-FORMED THIN-WALLED STEEL WITH SELF-DRILLING SCREW-PULL RIVET HYBRID CONNECTION

Yun-Peng Chu, Ming-Bo Huang *, Xue-Qin Chen and Jin-Rong Fu

*School of Civil Engineering and Architecture, Southwest University of Science and Technology, Mianyang 621010, China*

** (Corresponding author: E-mail: 1017325279@qq.com)*

**ABSTRACT**

This paper investigated the effects of corrosion on the shear performance of cold-formed thin-walled steel connections. Two types of connections were studied, specifically the pure self-drilling screw connection and the self-drilling screw-pull rivet hybrid connection. 120 cold-formed thin-walled steel connection specimens accelerated by the outdoor periodic automatic spray salt spray test were subjected to the shear test. The failure mode, shear capacity, and load-displacement curve were obtained. Subsequently, the test results were compared with those of the uncorroded specimens. The results indicated a significant degradation in the mechanical properties of the connection plate due to the corrosion. As the weight loss rate increased, a linear decrease occurred. Under the same weight loss rate, the shear capacity of the pure self-drilling screw connection decreased more than that of the self-drilling screw-pull rivet hybrid connection. This phenomenon became more obvious with the increase of ageing time. When the weight loss rate was 25.1%, the shear capacity of the 0.8 mm pure self-drilling screw connection decreased by 17.89%, while the self-drilling screw-pull rivet connection decreased by only 7.24%. The calculation equation of the shear capacity for pure self-drilling screw connections and self-drilling screw-pull rivet hybrid connections under the condition of corrosion damage were obtained. This calculation provided a reference for determining the shearing capacity of corrosion-damaged connections.

**ARTICLE HISTORY**

Received: 25 July 2025
Revised: 11 November 2025
Accepted: 12 November 2025

**KEYWORDS**

Corroded cold-formed thin-walled steel connection;
Shear test;
Shear capacity;
Calculation method



## 1. Introduction

Cold-formed thin-walled steel (CFS) structures commonly employ various connection methods, including screws, bolts, rivets, welding, and nails. Among these, self-drilling screws are widely utilized in CFS joint systems and component assembly due to their sufficient stiffness, strength, and deformability. The reliability of connection capacity is crucial for ensuring the overall structural integrity. However, when CFS components undergo significant corrosion under environmental exposure [1-2], degradation in connection strength and deterioration of mechanical properties in steel plates occur [3-7], ultimately compromising structural safety and durability.

Existing research on CFS connections has primarily focused on the shear behavior and capacity of uncorroded specimens [8-10]. Nevertheless, investigations into corroded CFS connections remain limited, despite corrosion being a prevalent environmental factor. The shear performance of such connections is governed by two key aspects: the mechanical properties of the connecting plates and the strength of the fasteners. The formation of irregular corrosion pits during the corrosion process significantly influences the mechanical behavior of steel plates [11-13].

Previous studies on corroded steel and CFS have established fundamental understanding of corrosion mechanisms and mechanical property degradation, yet they differ substantially from the present focus. Si et al. [14-17] demonstrated the dependence of mechanical properties on the complex apparent morphology of corroded steel plates. Zhang et al. [18]investigated fracture behavior in corroded CFS through micromechanical modeling, systematically characterizing the distribution and evolution of fracture parameters. Xu et al. [19] conducted experimental studies on CFS and hot-rolled steel subjected to long-term industrial service, revealing inferior ductility and toughness in corroded CFS compared to hot-rolled steel, with cold-working effects significantly influencing ductility. Qin et al. [20] analyzed the degradation of mechanical properties in corroded steel plates, noting minimal reduction in yield strength, ultimate strength, and fracture strength at mass loss rates below 15%, but significant deterioration beyond this threshold. Roy et al. [21] compared shear performance between corroded and uncorroded self-drilling screw connections, observing substantial strength reduction in corroded specimens. While addressing screw connection corrosion, their work considered neither hybrid connection systems nor comprehensive methods for calculating post-corrosion shear capacity.

The lightweight and flexible nature of CFS building structures, combined with extensive use of self-drilling screws in component-to-joist connections, creates vulnerability to wind-induced vibrations. Such dynamic loading can lead to connection loosening, screw hole enlargement, and eventual fastener pull-out, resulting in panel detachment from joists. These issues not only reduce load-bearing capacity and affect durability but may also cause severe structural damage upon entering the elastoplastic stage. Furthermore, the thin-walled nature of CFS sections makes them particularly susceptible to bearing capacity deterioration from corrosion, while reduced interlocking action between screw threads and corroded hole walls increases damage susceptibility.

To address these challenges, this study proposes implementing self-drilling screw-blind rivet hybrid connections as an alternative to conventional pure screw connections. Departing from previous research, we designed 30 groups totaling 120 corroded CFS connection specimens considering variables of connection plate thickness, connection type, and aging duration. Through shear tests examining failure modes, shear capacity, and load-displacement relationships, coupled with regression analysis of experimental data, this study establishes calculation methods for shear capacity in both pure self-drilling screw and hybrid connections under corrosion conditions. This approach addresses the limitation of previous single-connection-type studies and provides valuable reference for safety assessment of corroded connections.

## 2. Experimental investigations

### *2.1. Test specimen design*

Based on the Salt spray test for artificial atmosphere corrosion test (GB/T10125-2012) [22], the specimens were accelerated to a standard outdoor periodic automatic spray salt spray test. The salt fog had a chemical composition of 5% NaCl solution. The specimen was positioned in the testing groove at a 30-degree angle from the vertical direction (Fig. 1). All specimens were connected by connectors and then putted into the corrosion tank. All the steel of the connection was Q235B galvanized sheet. According to the different types of connectors, the specimens were divided into pure self-drilling screw connection (single connection) and self-drilling screw-pull rivet connection (hybrid connection). The self-drilling screw (see Fig. 2a) adopts ST4.2 cross countersunk head type, with a diameter of 4.2 mm. The open flat-headed pull rivet (see Fig. 2b) has a diameter that is approximately 4 mm, which is similar to that of the self-drilling screw. Both the self-drilling screw and the pull rivet are 16 mm in length. Based on the thickness of the connection plate, connection mode, and ageing time, 120 groups corroded CFS connection specimens were designed, each group having at least 4 identical specimens. The dimensions of the specimens are shown in Fig. 3, and the parameters are shown in Table 1.

**Table 1**
Basic parameters of specimens

| Group | Specimen number | Ageing time /day | t/mm | Connection mode |
|---|---|---|---|---|
| 1 | 2-0.8-d | 60 | 0.8+0.8 | single connection |
| 2 | 4-0.8-d | 120 | 0.8+0.8 | single connection |
| 3 | 6-0.8-d | 180 | 0.8+0.8 | single connection |
| 4 | 2-0.8-h | 60 | 0.8+0.8 | hybrid connection |
| 5 | 4-0.8-h | 120 | 0.8+0.8 | hybrid connection |
| 6 | 6-0.8-h | 180 | 0.8+0.8 | hybrid connection |
| 7 | 2-1.0-d | 60 | 1.0+1.0 | single connection |
| 8 | 4-1.0-d | 120 | 1.0+1.0 | single connection |
| 9 | 6-1.0-d | 180 | 1.0+1.0 | single connection |
| 10 | 2-1.0-h | 60 | 1.0+1.0 | hybrid connection |
| 11 | 4-1.0-h | 120 | 1.0+1.0 | hybrid connection |
| 12 | 6-1.0-h | 180 | 1.0+1.0 | hybrid connection |
| 13 | 2-1.2-d | 60 | 1.2+1.2 | single connection |
| 14 | 4-1.2-d | 120 | 1.2+1.2 | single connection |
| 15 | 6-1.2-d | 180 | 1.2+1.2 | single connection |
| 16 | 2-1.2-h | 60 | 1.2+1.2 | hybrid connection |
| 17 | 4-1.2-h | 120 | 1.2+1.2 | hybrid connection |
| 18 | 6-1.2-h | 180 | 1.2+1.2 | hybrid connection |
| 19 | 2-1.5-d | 60 | 1.5+1.5 | single connection |
| 20 | 4-1.5-d | 120 | 1.5+1.5 | single connection |
| 21 | 6-1.5-d | 180 | 1.5+1.5 | single connection |
| 22 | 2-1.5-h | 60 | 1.5+1.5 | hybrid connection |
| 23 | 4-1.5-h | 120 | 1.5+1.5 | hybrid connection |
| 24 | 6-1.5-h | 180 | 1.5+1.5 | hybrid connection |
| 25 | 2-2.0-d | 60 | 2.0+2.0 | single connection |
| 26 | 4-2.0-d | 120 | 2.0+2.0 | single connection |
| 27 | 6-2.0-d | 180 | 2.0+2.0 | single connection |
| 28 | 2-2.0-h | 60 | 2.0+2.0 | hybrid connection |
| 29 | 4-2.0-h | 120 | 2.0+2.0 | hybrid connection |
| 30 | 6-2.0-h | 180 | 2.0+2.0 | hybrid connection |

**Fig. 1** Specimen corrosion site

(a) (b)

**Fig. 2** The connector physical diagram: (a) The self-drilling screw; (b) The pull rivet

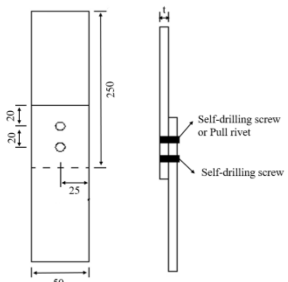


**Fig. 3** Connection mode

## 2.2. Tensile test

Under the erosion of chloride ion (cl-), the length of erosion time resulted in different corrosion degrees in the steel connections. The connection plates in the corroded CFS single and hybrid connection specimens with different thicknesses were cleaned using a 12% hydrochloric acid solution, followed by rinsing with water and neutralizing with lime water. Finally, the connection plates were rinsed with water and dried before being cut into 3 standard specimens for tensile test. The standard material specimen size is shown in Fig. 4. The weight loss rate of the specimen could be used as the quantitative index to measure the degree of corrosion. The relationship between the weight loss rate and the ageing time of various steel thicknesses is shown in Fig. 5. It can be seen that under the same ageing time, the weight loss rate increases as the thickness of the connection plate becomes smaller. On the other hand, the thicker the plate, the less prone it is to corrosion. As the ageing time increases, the weight loss rate of connection plates with smaller thicknesses increases significantly. The weight loss rate can be determined using Eq. (1).

$$\eta=\frac{m_0-m_1}{m_0}\times 100\% \tag{1}$$

where $\eta$ is the weight loss rate, $m_0$ is the mass of the specimen before corrosion, and $m_1$ is the mass of the specimen after corrosion removal and drying.

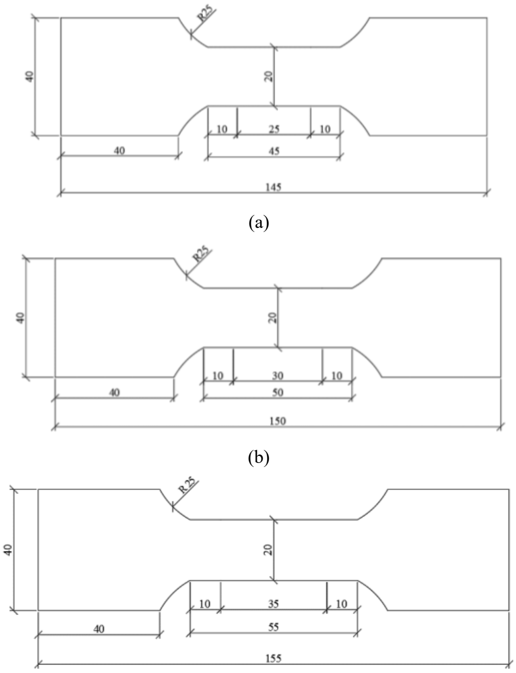


**Fig. 4** The standard material specimen size: (a) The thickness of the connecting plate is 0.8 mm and 1.0 mm; (b) The thickness of the connecting plate is 1.2 mm and 1.5 mm; (c) The thickness of the connecting plate is 2.0 mm

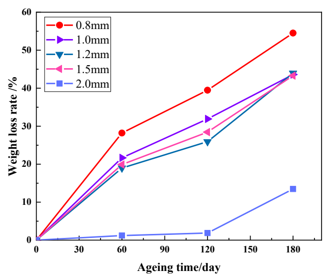


**Fig. 5** The relationship between ageing time and weight loss rate of connection plate.

The tensile test was carried out in the universal testing machine. According to Metallic Materials-Tensile testing-Part 1: Method of test at room temperature (GB/T228.1-2010) [23], the loading rate of the elastic stage and the yield stage is 0.75 mm/min. The loading rate of hardening stage is set to 5 mm/min. The mechanical properties of a material can be determined through the tensile test. If there is no clear yield point in the specimen, the stress at 0.2% plastic deformation is considered as the yield strength. Fig. 6 presents the stress-strain curve and Table 2 shows the main performance indicators. The weight loss rate and main performance indicators are the mean values of the measurement results of the standard specimens of each thickness.

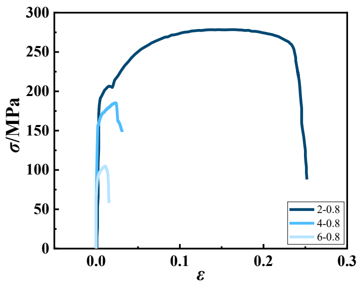


(a)

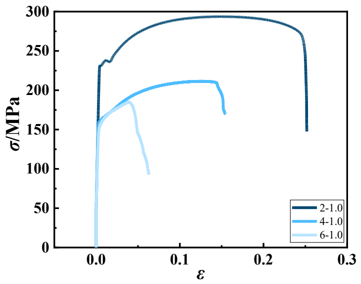


(b)

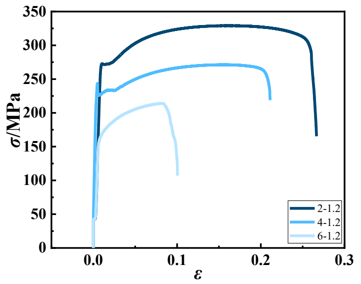


(c)

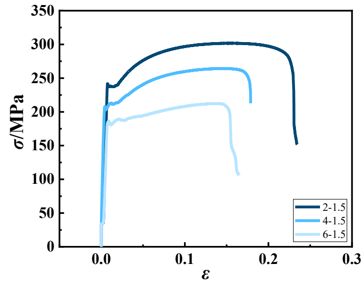


(d)

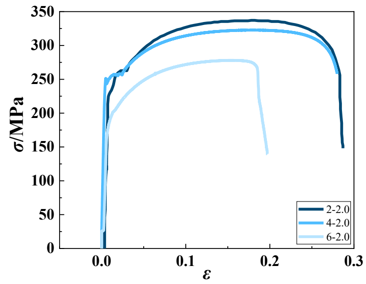


(e)

**Fig. 6** Stress-strain curves of connection plate specimens in different ageing time: (a) 0.8 mm plate, (b) 1.0 mm plate, (c) 1.2 mm plate, (d) 1.5 mm plate, (e) 2.0 mm plate

As can be seen from Fig. 6, the stress-strain curve of specimens with less weight loss rate still exhibits four typical stages. As the weight loss rate increases, the elastic stage of each specimen becomes shorter and the slope decreases. During the yield stage, the yield platform significantly shortens or disappears due to the stress concentration caused by local etch pits on the surface of the connection plate, and the material enters the plastic stage prematurely. This trend becomes more noticeable as the weight loss rate increases. The peak load during the strengthening stage decreases as the weight loss rate increases. The necking stage also decreases with an increased weight loss rate and disappears once a certain corrosion degree is reached. According to Table 2, the mechanical properties of the connetion plates decline as the ageing time increases. Fu et al. [24] studied the mechanical properties of CFS hybrid connection double-limb composite members through experiments. The basic data of uncorroded specimens in this paper refer to this study.

**Table 2**
Material mechanical test results (Note: 1GPa=1000MPa)

| t (mm) | Ageing time（day） | Yield strength（MPa） | Ultimate strength（MPa） | Elastic modulus（GPa） | Weight loss rate（%） | Elongation（%） |
|---|---|---|---|---|---|---|
| 0.8 | 0 [24] | 272.5 | 360.3 | 200 | 0 | 30.7 |
| | 60 | 195.2 | 277.5 | 126.31 | 28.20 | 25.1 |
| | 120 | 156.3 | 185.2 | 104.32 | 39.47 | 3.1 |
| | 180 | 81.4 | 104.7 | 79.78 | 54.51 | 1.5 |
| 1.0 | 0 [24] | 259.6 | 358.2 | 204 | 0 | 32.8 |
| | 60 | 230 | 293.7 | 131.4 | 21.66 | 25.2 |
| | 120 | 164.2 | 211.4 | 99.27 | 35.76 | 15.5 |
| | 180 | 152.7 | 185.1 | 82.63 | 43.60 | 6.3 |
| 1.2 | 0 [24] | 288.2 | 353.4 | 206 | 0 | 29.5 |
| | 60 | 272.5 | 329.2 | 142.5 | 18.98 | 26.7 |
| | 120 | 225.6 | 271.3 | 130.3 | 25.93 | 21.1 |
| | 180 | 145.1 | 214.1 | 89.9 | 43.98 | 10.1 |
| 1.5 | 0 [24] | 263.2 | 355.1 | 213 | 0 | 30.5 |
| | 60 | 235 | 301.7 | 140.9 | 19.98 | 23.4 |
| | 120 | 202.9 | 264.6 | 125.6 | 28.44 | 17.9 |
| | 180 | 165.1 | 212.4 | 94.9 | 43.31 | 16.5 |
| 2 | 0 [24] | 262.4 | 365.8 | 210 | 0 | 31.2 |
| | 60 | 256.2 | 345.7 | 199.6 | 1.20 | 28.7 |
| | 120 | 244.1 | 322.8 | 185.0 | 1.87 | 28.0 |
| | 180 | 210.5 | 280.2 | 161.4 | 13.47 | 19.7 |

### 2.3. Degradation rule of mechanical properties

To study the degradation of mechanical properties for connection plates with different ageing times. The weight loss rate was used as a quantitative index for the regression analysis of tensile test value in this paper. The relationship between the yield strength, ultimate strength, elastic modulus, elongation, and the weight loss rate of the steel with different ageing times was obtained (Fig. 7).

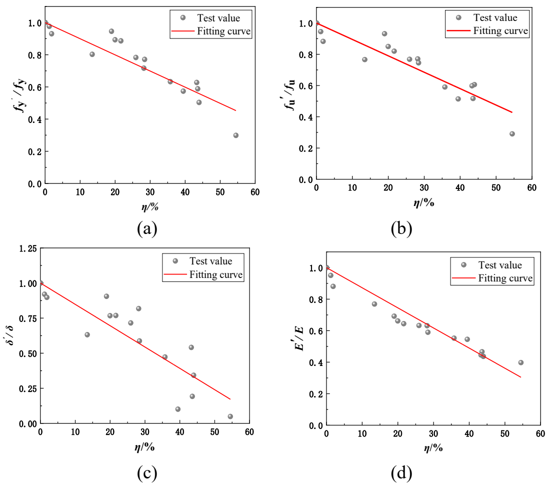


**Fig. 7** Relationship between material mechanical and weight loss rate: (a) the yield strength, (2) ultimate strength, (c) elongation, (d) elastic modulus

It can be seen from Fig. 7 that there is an approximately linear relationship between the mechanical properties of the steel and the weight loss rate under different ageing times. The performance indices show different degrees of deterioration as the weight loss rate increases. The mathematical expressions are as follows:

$$f_y^{'}/f_y = 1 - 0.01004\eta \tag{2}$$

$$f_u^{'}/f_u = 1 - 0.0105\eta \tag{3}$$

$$\delta^{'}/\delta = 1 - 0.152\eta \tag{4}$$

$$E^{'}/E = 1 - 0.01277\eta \tag{5}$$

in which, $f_y$, $f_u$, $\delta$, $E$, and $f_y'$, $f_u'$, $\delta'$, $E'$ are the yield strength, ultimate strength, elongation and elastic modulus of steel before and after corrosion, respectively.

### 2.4. Test device and loading system

The loading control and data acquisition were performed by a universal testing machine, and the loading device was shown in Fig. 8. Loading was controlled by the displacement at a rate of 2.5 mm/min. Before loading, the fixtures at both ends were adjusted to ensure that the force of the specimen remained in a straight line.

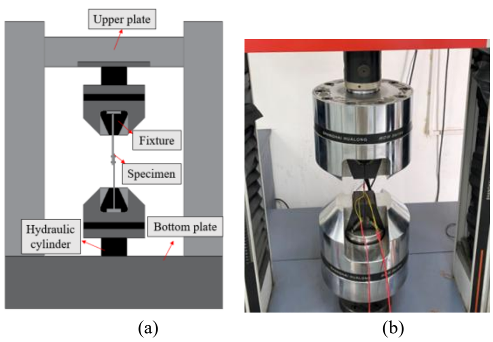


**Fig. 8** Schematic diagram of loading device: (a) Loading device schematic, (b) Loading device real shot

## 3. Test result

### 3.1. Surface morphology of corroded connection plate

The surface morphology of connection plates before and after corrosion removal in varying ageing times is illustrated in Fig. 9. The corrosion layer on the connection plate, which had been subjected to 60 days of corrosion, was relatively light and thin with an orange hue. Following the removal of the corrosion, the surface of the connection plate exhibited small etch pits. The corrosion layer on the surface of the connection plate thickened and turned orange or reddish brown after 120 days. A slight scrape could remove a fraction of the corroded layer, and a small area of scab was locally distributed on the surface. After removing corrosion, the number of etch pits on the surface of connection plate rose, and certain neighboring etch pits showed a tendency to fuse. After 180 days of corrosion, the corrosion layer on the surface of the connection plate was brown. There was hollowing between the corrosion layer and the base material in certain areas. When touched lightly, the corrosion fell off in large areas. After the removal of the corrosion, most of the nearby etch pits combined to form larger etch pits.

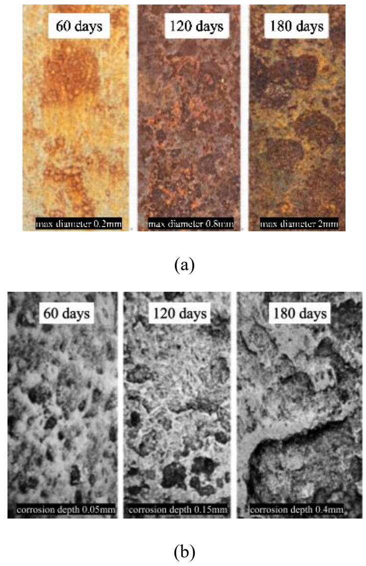


**Fig. 9** Surface morphology of connection plate with different ageing times: (a) Before corrosion removal, (b) After corrosion removal

### 3.2. failure mode

#### 3.2.1. Single connection

The failure modes of the single connection specimens were shown in Fig. 10, respectively. At the initial loading, there was no obvious deformation of the specimen. However, as the load gradually increased, the specimen entered into a plastic stage and the self-drilling screws began to inclined. As the load was increased to the ultimate load, the inclination of the self-drilling screw was exacerbated, and the self-drilling screw of some specimens appeared to be gradually stripped. Concurrently, the specimen emitted a sound of "da da da". In the final stage of the test, the self-drilling screws were pulled out, the nail holes were enlarged, and the plate connection failed. The aging time was 180 days, and the thickness of the connecting plate was 0.8mm and 1.0mm. When the specimen was destroyed, it was more likely to tear the connecting plate and cause it to be unable to continue to bear the load.

The failure modes of the uncorroded single connection specimen [24] were primarily as follows: (1) When the thickness of the connecting plate was thin, the screw became inclined with the loading and was quickly pulled off due to the enlargement of the pressure hole in the plate. (2) The screw was pulled off during shear process, resulting in a decrease in bearing capacity. However, deformation of the connecting plate was relatively small. (3) The 2.0mm connection specimen experienced very little deformation, and ultimately had its screw cut off.

The change in failure mode of the connecting specimen before and after corrosion could be attributed to several factors including thinning of connecting plate thickness, deterioration of mechanical properties, reduction in diameter of connecting piece, and enlargement of nail hole.

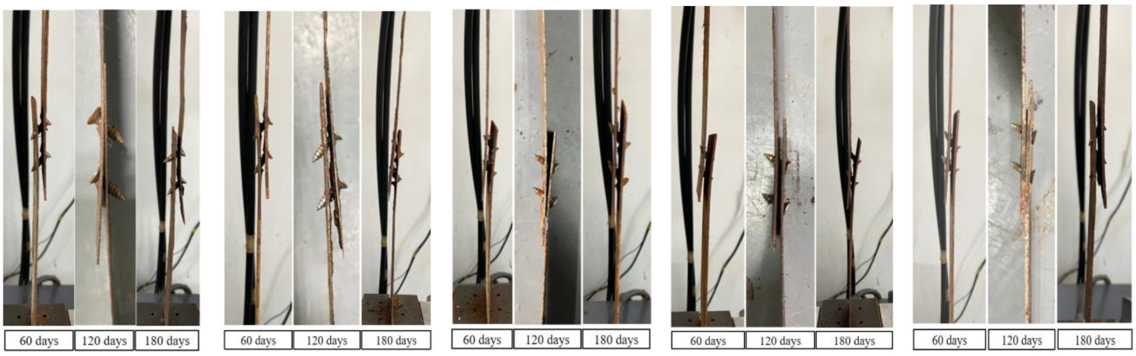


(a) (b) (c) (d) (e)

**Fig. 10** Single connection failure mode: (a) 0.8mm; (b) 1.0mm; (c) 1.2mm; (e)1.5mm; (f)2.0mm

*3.2.2. Hybrid connection*

The failure modes of the hybrid connection specimens were illustrated in Figure 11, respectively. During the initial loading stage, the hybrid connection specimens exhibited the same mechanical behaviors as the single connection specimens with increasing load. For specimens with connecting plate thicknesses of 0.8 mm, 1.0 mm, and 1.2 mm, the inclination angle of the self-tapping screws increased significantly. Among these, specimens with an aging time of 120 days and 180 days showed a notable increase in the spacing between connecting plates, which was attributed to the enlargement of screw hole diameters caused by corrosion and the mechanical stress acting on the surrounding plate surfaces. It is noteworthy that the inclination angles of specimens with connecting plate thicknesses of 1.5 mm and 2 mm were lower than those of the aforementioned specimens. This is because the larger thickness of the connecting plates, combined with the presence of blind rivets that firmly locked the connecting plates, restricted the inclined deformation of the screws to a certain extent. At the ultimate load, the overall performance of the specimen was characterized by the bearing failure on the surface of the connecting plate surrounding the nail hole and the warping of the plate end. According to the final failure mode diagram, the inclination of self-drilling screws and pull rivets increased significantly in the specimens with an aging time of 120 and 180 days compared to those with an aging time of 60 days. Additionally, the spacing between connecting plates also increased.

The hybrid connection specimens with connecting plate thicknesses of 1.5 mm and 2 mm showed no obvious deformation at the initial loading stage. As the load increased, the screw gradually inclined and the end of the plate began to warp. Notably, its inclination was lower than that of the hybrid connection specimens with connecting plate thicknesses of 0.8 mm, 1.0 mm, and 1.2 mm. This is due to the connection plate thickness is large, and the presence of pull rivets firmly locked the connection plate, to a certain extent, to limit the screw inclined deformation. At the ultimate load, connecting plate thickness of 1.5mm and 2.0mm specimens produce a "bang" sound, pull rivets were sheared, connecting plate around the nail holes plate surface bearing damage accompanied by the end of the plate warping.

The failure modes of uncorroded hybrid connection specimens [24] can be classified into two primary categories: (1) Hybrid connection specimens with plate thicknesses of 0.8mm, 1.0mm, and 1.2mm exhibited a failure mode in which the connection plate underwent pressure failure, accompanied by screw tilt failure. (2) Specimens with plate thicknesses of 1.5mm and 2mm exhibited a failure mode in which the pull-rivets were cut off, and the deformation of the specimens was small.

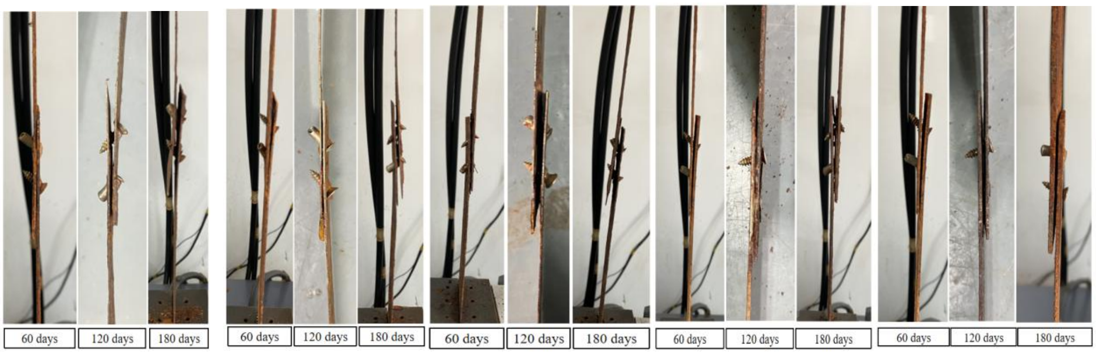


(a) (b) (c) (d) (e)

**Fig. 11** Hybrid connection failure mode: (a) 0.8mm; (b) 1.0mm; (c) 1.2mm; (e)1.5mm; (f)2.0mm

*3.3. Load-displacement curve*

The load-displacement curve is shown in Fig.12. Overall, the failure process of the connecting specimens had certain common characteristics. During the initial stage of loading, the load-displacement curves of each specimen were linear. The displacement of the connecting specimens with different ageing times did not change significantly with increasing load. However, once the load exceeded a critical limit, a sudden displacement occurred, which became more evident with longer ageing times. This was caused by the brittle bonding effect of corrosion products between the self-drilling screw, the pull rivet, and the connection plate. When the load was below a certain value, the self-drilling screw and the pull rivet bore minimal workload. Nevertheless, when the bonding effect failed, the connector was forced to bear the load.

When the load continues to increase, the curve gradually transits from linear to nonlinear. The slope of the curve exhibited increasing trends followed by decreasing trends. As the weight loss rate increases, the etch pits on the surface of the connection plate become more complex, and stress concentration intensifies. This results in a rapid transition of the steel plate into the plastic stage. Consequently, an observable bending of the load-displacement curve occurred. When the curve entered the plastic stage, the load-displacement curve tended to be gentle, and the deformation of the specimen connection area intensified.

In the latter phase of loading, The connection plate thickness was 0.8mm, 1.0mm and 1.2mm specimen stiffness decreased due to the self-drilling screws' inclination. The interlocking effect betwen the self-drilling screw's thread and the connection plate's hole wall enabled the specimens to continue supporting the increased external load. However, when the interlocking effect between the self-drilling screw's thread and the plate's hole wall could not resist the increasing external load, the screw slid off the plate. These caused the load-displacement curve to fluctuate in a wavy manner. The performance of the single connection specimen became more pronounced. However, For the specimens with connection plate thicknesses of 1.5 mm and 2.0 mm, the self-drilling screws of the corroded single connection specimens exhibit pull-off failure when the load reached the shear capacity. This is due to the relatively large thickness of the connection plate and the enlarged holes caused by the corrosion. Among them, the thickness of the connection plate for 4-1.5-d and 6-1.5-d decreased due to corrosion. It could seen that the load-displacement curve also exhibited a more obvious wave-line trend. The pull rivets of the hybrid connection specimens were cut off after reaching the shear capacity, causing a sudden drop in load and resulting in brittle fracture.

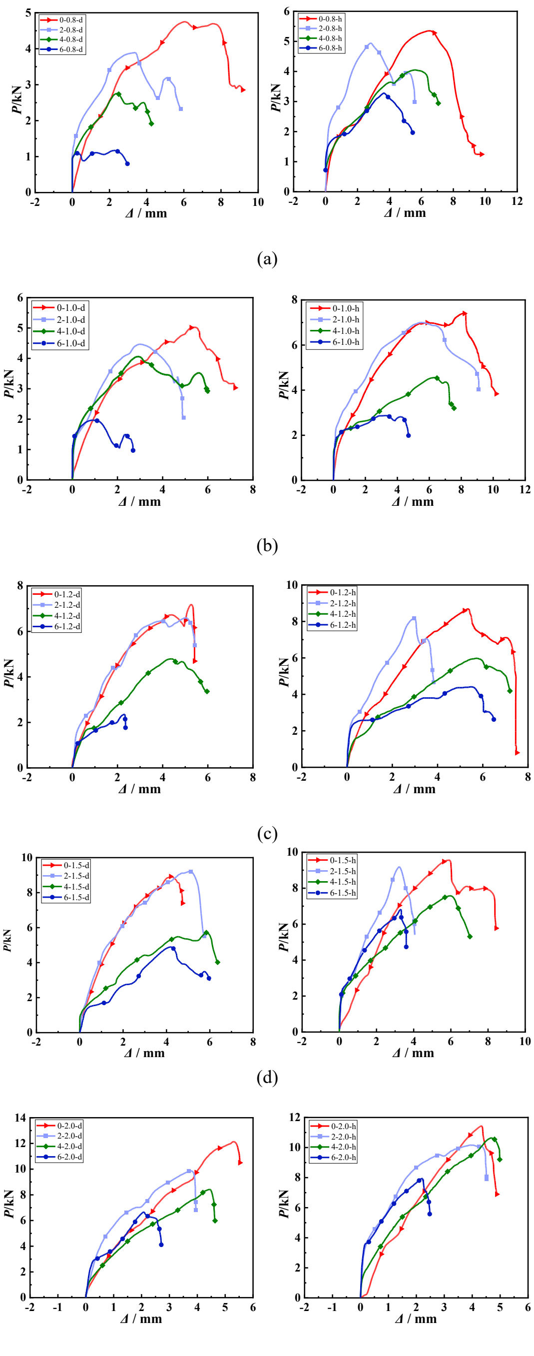


**Fig. 12** Load-displacement curve of corroded specimen for different thickness of the connecting plate: (a) 0.8mm. (b) 1.0mm. (c) 1.2mm, (d) 1.5mm, (e) 2.0mm

### *3.4. Analysis of shear capacity*

Table 3 and 4 was the test value of shear capacity with different ageing time. The test results indicate that there was no significant difference between the test values of the uncorroded single connection and the hybrid connection. However, as the ageing time increased, the shear capacity of the single connection specimen with the same thickness decreased considerably when compared to the hybrid connection specimen. This indicated that the self-drilling screws were more prone to corrosion than the pull rivet.

Compared to the uncorroded specimens, the shear capacity for single connection specimens with connection plate thickness of 0.8 mm decreased by 17.89%, 43.15%, and 74.74% respectively, as the ageing time increased. Similarly, the shear capacity of hybrid connection specimens decreased by 7.24%, 24.86%, and 38.78% respectively. For single connection specimens with connection plate thickness of 1.0 mm, the shear capacity decreased by 11.33%, 23.86%, and 60.24% respectively, while that of the hybrid connection specimens decreased by 5.79%, 38.63%, and 60.97% respectively. The shear capacity for single connection specimens with connection plate thickness of 1.2 mm decreased by 8.08%, 33.01%, and 66.57% respectively, and that of hybrid connection specimens decreased by 8.15%, 31.57%, and 51.21% respectively. Moreover, the shear capacity for single connection specimens with connection plate thickness of 1.5 mm decreased by 7.53%, 35.83%, and 45.13% respectively, while that of the hybrid connection specimens decreased by 4.81%, 20.92%, and 37.24% respectively. Finally, the shear capacity for single connection specimens with connection plate thickness of 2.0 mm decreased by 22.98%, 32.95%, and 44.81% respectively, and that of hybrid connection specimens decreased by 10.76%, 17.76%, and 30.88% respectively.

Owing to the galvanization and passivation treatments applied to blind rivets, their corrosion rate in salt spray tests is lower than that of self-tapping screws. In hybrid connections, blind rivets bear part of the shear force, which reduces the stress on self-tapping screws and mitigates the risks of screw hole enlargement and screw pull-out. Additionally, the locking effect of blind rivets on connecting plates inhibits the increase in inter-plate gaps caused by corrosion and alleviates stress concentration. Therefore, compared with single-type connections, hybrid connections are more effective in resisting corrosion-related degradation.

**Table 3**
Test value of shear bearing capacity of single connection (unit: kN)

| Specimen number | 0 day [24] | 60 days | 120 days | 180 days |
|---|---|---|---|---|
| 0.8-d | 4.75 | 3.90 | 2.7 | 1.20 |
| 1.0-d | 5.03 | 4.46 | 3.83 | 2.00 |
| 1.2-d | 7.18 | 6.60 | 4.81 | 2.40 |
| 1.5-d | 8.93 | 8.30 | 5.73 | 4.90 |
| 2.0-d | 12.14 | 9.35 | 8.44 | 6.70 |

**Table 4**
Test value of shear bearing capacity of hybrid connection (unit: kN)

| Specimen number | 0 day [24] | 60 days | 120 days | 180 days |
|---|---|---|---|---|
| 0.8-h | 5.39 | 5.00 | 4.05 | 3.30 |
| 1.0-h | 7.43 | 7.00 | 4.56 | 2.90 |
| 1.2-h | 8.71 | 8.00 | 5.96 | 4.25 |
| 1.5-h | 9.56 | 9.10 | 7.56 | 6.00 |
| 2.0-h | 11.43 | 10.20 | 9.4 | 7.90 |

## 4. Calculation method of shear capacity

For the connection that uses one self-drilling screw connected, the calculation method outlined in the GB 50018-2002 has been deemed too conservative [25]. As such, the method of calculating shear capacity for hybrid connections utilizes the North American specification [27] to calculate the shear capacity of a single screw connection. At the same time, referring to the calculation method of the shear capacity for the rivet connection in the European standard EN1993-1-3 [28] , the rivet part in the hybrid connection is calculated. The sum of the two values is the shear capacity of the hybrid connection (see Eq. 6). The results are shown in Table 5, it can be seen that the calculation results are too conservative, so it is improved.

When analyzing the failure modes of hybrid connections, it is clear that damage to the surface of the connecting plate under pressure leads to deformation of the plate, inclination of the screws, and increased spacing between the plates. This, in turn, leads to an increased risk of pull-off for the screws. However, the rivet can prevent the increase of plate distance, and the rivet has a tendency to cut. It is worth noting that the self-drilling screw offers greater shear strength and can limit the shear of the pull rivet in this context. The shear capacity is influenced by the self-drilling screw screw and pull rivet connections. When the shear failure of the pull rivet occurs, the pull rivet is cut before the self-drilling screw, and this failure mode mainly occurs in the connection with larger thickness of the composite plate. Based on this, the failure mode is combined with the calculation of shear capacity, and the calculation method of shear capacity under different failure modes after the hybrid connection of rivet and self-drilling screw is modified. When the thickness of the composite plate $t_1 + t_2 < 3$mm, the shear capacity of the hybrid connection $P_h$ is determined by Eq. (7). When the thickness of the composite plate $t_1 + t_2 \geq 3$mm, $P_h$ is determined by Eq. (8). The calculation results of shear capacity before and after improvement are shown in Table 5.

Based on the provisions in Section 8 of the North American specification AISI S100-16 [27] for the shear capacity calculation method of a single self-drilling screw connection, and the shear capacity calculation method for riveted connections specified in the European standard EN 1993-1-3 [28], an improved shear capacity calculation formula for the hybrid joint was proposed：

The shear capacity of the hybrid connection before improvement:

$$P_{\mathrm{m}} = F_{\mathrm{b}} + P_{\mathrm{ns}} \tag{6}$$

The shear capacity of the hybrid connection after improvement:

$$P_{\mathrm{h}} = \varphi\left(F_{\mathrm{b}} + P_{\mathrm{ns}}\right) \tag{7}$$

$$P_{\mathrm{h}} = F_{\mathrm{b}} + \lambda P_{\mathrm{ns}} \tag{8}$$

in which, $\varphi$ and $\lambda$ are the influence factor coefficient of shear capacity for single screw, taking as $\varphi$=1.5, $\lambda$=1.13 [24], $P_{ns}$ [27], $F_b$ [28].

**Table 5**
Calculation results of shear capacity for uncorroded hybrid connection

| t/mm | $P_{\mathrm{m}}$ | $P_{\mathrm{h}}$ | $P_{\mathrm{t}}$ | $P_t/P_{\mathrm{m}}$ | $P_t/P_{\mathrm{h}}$ |
|---|---|---|---|---|---|
| 0.8+0.8 | 3.54 | 5.28 | 5.39 | 1.52 | 1.02 |
| 1.0+1.0 | 4.92 | 7.21 | 7.43 | 1.51 | 1.03 |
| 1.2+1.2 | 6.38 | 9.90 | 8.71 | 1.37 | 0.88 |
| 1.5+1.5 | 8.96 | 12.58 | 9.56 | 1.07 | 0.76 |
| 2.0+2.0 | 13.21 | 11.66 | 11.43 | 0.87 | 0.98 |
| Average | - | - | - | 1.27 | 0.93 |

After comparing the test results and the calculated values in Table 5, it is evident that there is a significant difference between the calculated and test results before the improvement. The average values of the ratio of the calculated value to the test value of the shear capacity of the uncorroded hybrid connection, calculated by the before and after improved method, are 1.27 and 0.93, respectively. The difference between the calculated value and the test value is minimal. It can be concluded that this calculation method is more reasonable than the direct accumulation method.

As the weight loss rate increases, the shear capacity of CFS single connection and hybrid connection gradually decreases. The corrosion of both the plate and the connectors affects the shear capacity, and the degree of corrosion is different. Therefore, the discreteness of the shear capacity value is large. To account for the impact of connector corrosion, we introduce a corrosion factor $\varepsilon$ to modify the equation above. The shear bearing capacity of the corroded specimens is $P_c$. The shear capacity of the connection specimen after thickness reduction is represented by $P_t$, which is calculated based on the corresponding corrosion rate. The influence factor calculation equation is obtained by fitting the test data. The $R^2$ of single connection is 0.8899 and 0.9115, respectively. The $R^2$ of hybrid connection is 0.873 and 0.9789, respectively. The results are shown in Table (6) and Table (7).

$$P_{\mathrm{c}} = \varepsilon P_t \tag{9}$$

Single connection:

$$\varepsilon = \begin{cases} 0.4976\mathrm{e}^{0.0394\eta} & \eta \le 40\% \\ 0.0784e^{0.0784\eta} & \eta > 40\% \end{cases} \tag{10}$$

Hybrid connection:

$$\varepsilon = \begin{cases} 0.6433e^{0.0362\eta} & \eta \le 40\% \\ 0.0132e^{0.1148\eta} & \eta > 40\% \end{cases} \tag{11}$$

**Table 6**
Calculation results of shear capacity for CFS single connection

| t (mm) | Ageing time (day) | Weight loss rate (%) | $P_{\mathrm{c}}$ (kN) | $P_{\mathrm{t}}$ (kN) | $P_c/P_t$ |
|---|---|---|---|---|---|
| 0.8 | 60 | 28.20 | 3.52 | 3.90 | 0.90 |
| | 120 | 39.47 | 2.62 | 2.70 | 0.97 |
| | 180 | 54.51 | 1.05 | 1.20 | 0.88 |
| 1.0 | 60 | 21.66 | 4.17 | 4.46 | 0.93 |
| | 120 | 35.76 | 3.12 | 3.83 | 0.81 |
| | 180 | 43.60 | 2.36 | 2.00 | 1.18 |
| 1.2 | 60 | 18.98 | 6.39 | 6.60 | 0.97 |
| | 120 | 25.93 | 5.55 | 4.81 | 1.15 |
| | 180 | 43.98 | 3.31 | 2.40 | 1.38 |
| 1.5 | 60 | 19.98 | 8.72 | 8.30 | 1.05 |
| | 120 | 28.44 | 6.58 | 5.73 | 1.15 |
| | 180 | 43.31 | 4.24 | 4.90 | 0.87 |
| 2.0 | 60 | 1.20 | 9.16 | 9.35 | 0.98 |
| | 120 | 1.87 | 8.64 | 8.44 | 1.02 |
| | 180 | 13.47 | 6.85 | 6.70 | 1.02 |
| Average | - | - | - | - | 1.01 |

**Table 7**
Calculation results of shear capacity for CFS hybrid connection

| t（mm） | Ageing time (day) | Weight loss rate (%) | $P_{\mathrm{c}}$ （kN） | $P_t$（kN） | $P_c/P_t$ |
|---|---|---|---|---|---|
| 0.8 | 60 | 28.20 | 4.14 | 5 | 0.83 |
| | 120 | 39.47 | 3.51 | 4.05 | 0.87 |
| | 180 | 54.51 | 2.56 | 3.3 | 0.78 |
| 1.0 | 60 | 21.66 | 6.16 | 7 | 0.88 |
| | 120 | 35.76 | 5.14 | 4.56 | 1.13 |
| | 180 | 43.60 | 4.5 | 2.9 | 1.55 |
| 1.2 | 60 | 18.98 | 7.81 | 8 | 0.98 |
| | 120 | 25.93 | 6.88 | 5.96 | 1.15 |
| | 180 | 43.98 | 5.24 | 4.25 | 1.23 |
| 1.5 | 60 | 19.98 | 9.12 | 9.1 | 1.00 |
| | 120 | 28.44 | 7.32 | 7.56 | 0.97 |
| | 180 | 43.31 | 5.82 | 6 | 0.97 |
| 2.0 | 60 | 1.20 | 10.00 | 10.2 | 0.98 |
| | 120 | 1.87 | 9.62 | 9.4 | 1.02 |
| | 180 | 13.47 | 7.86 | 7.9 | 0.99 |
| Average | - | - | - | - | 1.01 |

From Table 6 and 7, it is evident that, except for individual specimens, the calculation results for the shear capacity of both the single connection and hybrid connection proposed in this paper correspond well with the test results. The ratio of theory to test obtained by the calculation method of shear capacity of single connection and hybrid connection proposed in this paper has an average value of 1.01. It can see that the equations proposed in this paper are consistent and accurate, and the accuracy is high. The proposed calculation method is capable of accurately predicting the shear capacity of both single and hybrid CFS connection specimens, which affected by corrosion.

## 5. Conclusions

In this paper, the shear test of CFS connection specimens under salt spray corrosion was carried out. The failure mode, shear capacity and load-displacement curve of CFS connection were analyzed. The following conclusions were drawn:

(1) Corrosion causes a clear degradation of the mechanical properties of the connection plate. The yield and tensile strengths decrease linearly with an increase in weight loss rate. Moreover, the elastic stage in the stress-strain curve becomes shorter, the yield point decreases, and the yield platform may even disappear.

(2) The reduction of the shear capacity in pure self-drilling screw connection specimens with various degrees of corrosion is greater compared to that of self-drilling screw-pull rivet hybrid connection specimens. Additionally, the longer the ageing time lasts, the more apparent the phenomenon becomes. For instance, when the weight loss rate is at 25.1%, the reduction rates for the pure self-drilling screw connection with a connection plate thickness of 0.8 mm and the self-drilling screw-pull rivet connection are 17.89% and 7.24%,

respectively.

(3) With the weight loss rate increases, there is no significant difference in the failure mode of the same series of specimens before and after corrosion. The specimens with self-drilling screw-pull rivet hybrid connection still fail due to rivet being cut off and plate bearing failure. The pure self-drilling screw connection specimens fail due to screw pull off and plate bearing failure.

(4) On the basis of the code, considering the corrosion effect of the connector, the corrosion factor is introduced to obtain the calculation equation of the shear capacity of the corroded cold-formed thin-walled steel connection. The ratio of theory to test obtained by the calculation method of shear capacity of single connection and hybrid connection proposed in this paper has an average value of 1.01. It indicates that the proposed method can forecast the shear capacity of pure self-drilling screw connection and self-drilling screw-pull rivet hybrid connection CFS specimens that have corroded more accurately.

## 6. Application guide for engineering design

Based on the test results and analytical findings, the following recommendations are proposed:

(1) In severe corrosive environments such as coastal areas and high-humidity regions, the self-tapping screw-blind rivet hybrid connection should be prioritized. The thickness of the connecting plate should not be less than 1.5 mm, considering that the bearing capacity of the 1.5 mm-thick plate decreases by 37.24% after 180 days of corrosion, which is significantly lower than the 74.74% reduction of the 0.8 mm-thick plate. (2) In dry and low-corrosion environments, the single self-tapping screw connection can be adopted. (3) Given that a 15% mass loss rate is the mutation point of mechanical properties, inspections should be conducted every 60 days in severe corrosive environments and every 120 days in moderate corrosive environments. When the mass loss rate exceeds 15%, timely replacement or reinforcement measures should be implemented.

## Acknowledgment

This study was financially supported by the National Natural Science Foundation of China (Grant No.52268029) and the Basic Research Project of Science and Technology Department of Sichuan Province (Grant no. 2023JDZH0035) and Natural Science Foundation of Sichuan Province (Grant No. 2023NSFSC0381).

## References

[1] L. Cascini, F. Portioli, R. Landolfo. Probabilistic time variant assessment of thin-walled steel members under atmospheric corrosion attack [J]. Journal of Civil Engineering and Management, 2014, 20(3): 404-414. https://doi.org/10.3846/13923730.2013.802709

[2] Z. Zhao, B. Liang, H. Liu, et al. Load capacity of corroded welded hollow spherical joints subjected to bending moment and axial force [J]. Journal of Building Engineering, 2019, 25: 100824. https://doi.org/10.1016/j.jobe.2019.100824

[3] S.H. Xu, H. Wang, L. Su. Degradation law of mechanical properties of Q235 steel plate in neutral salt spray corrosion environment [J]. Mater. Mech. Eng, 2016, 40(5): 86-91. (in Chinese)

[4] Y. Wang, S. Xu, H. Wang, et al. Predicting the residual strength and deformability of corroded steel plate based on the corrosion morphology [J]. Construction and Building Materials, 2017, 152:777-793. https://doi.org/10.1016/j.conbuildmat.2017.07.035

[5] S. Xu, Z. Zhang, R. Li, et al. Effect of cleaned corrosion surface topography on mechanical properties of cold-formed thin-walled steel [J]. Construction and Building Materials, 2019, 222: 1-14. https://doi.org/10.1016/j.conbuildmat.2019.06.130

[6] B. Nie, S. Xu, Z. Zhang, et al. Experimental investigation on corroded cold-formed steel beam-columns under compression and major axis bending [J]. Journal of Constructional Steel Research, 2020, 169: 106026. https://doi.org/10.1016/j.jcsr.2020.106026

[7] Z. Zhang, S. Xu, R. Li. Comparative investigation of the effect of corrosion on the mechanical properties of different parts of thin-walled steel [J]. Thin-Walled Structures, 2020, 146: 106450. https://doi.org/10.1016/j.tws.2019.106450

[8] R Serrette, D. Peyton. Strength of screw connections in cold-formed steel construction[J]. Journal of structural engineering, 2009, 135(8): 951-958. https://doi.org/10.1061/(ASCE)0733-9445(2009)135:8(951)

[9] J.P. Hao, B. Liu, D.Y. Zhao, et al. Experimental study on shear behavior of screw connections in cold-formed thin-wall steel structures [J]. Journal of Xi'an University of Architecture & Technology: Natural Science Edition, 2014, 46(6): 769-773 (in Chinese) https://doi.org/10.15986/j.1006-7930.2014.06.001

[10] Y. Guan, X.H. Zhou, X.M. Yao, et al. Experimental study on shear behavior of cold-formed thin-walled steel composite floor and self-tapping screw connection [J]. Journal of Civil Engineering, 2018,51 (10): 27-36 + 67. https://doi.org/10.15951/j.tmgcxb.2018.10.004.

[11] Y. WANG, S. XU, H. LI, et al. Surface characteristics and stochastic model of corroded structural steel under general atmospheric environment[J]. Acta Metall Sin, 2019, 56(2): 148-160. https://doi.org/10.11900/0412.1961.2019.00156

[12] A. Li, S. Xu, H. Wang, et al. Bond behaviour between CFRP plates and corroded steel plates [J]. Composite Structures, 2019, 220: 221-235. https://doi.org/10.1016/j.compstruct.2019.03.068

[13] S. Xu, H. Li, Y. Wang, et al. Influence of corrosion on the bond behavior in CFRP-steel single lap joints [J]. Construction and Building Materials, 2020, 236: 117607. https://doi.org/10.1016/j.conbuildmat.2019.117607

[14] Q. Si, Y. Ding, L. Zong, et al. Mechanical Behaviour of Corroded Structural Steel Subjected to Monotonic Tension [J]. Advanced Steel Construction, 2022, 18(3): 707-714. https://doi.org/10.18057/IJASC.2022.18.3.8

[15] G. Qin, S.Xu, D. Yao, et al. Study on the degradation of mechanical properties of corroded steel plates based on surface topography [J]. Journal of Constructional Steel Research, 2016, 125: 205-217. https://doi.org/10.1016/j.jcsr.2016.06.018

[16] Y. Wang, S. Xu, H. Wang, et al. Predicting the residual strength and deformability of corroded steel plate based on the corrosion morphology [J]. Construction and Building Materials, 2017, 152: 777-793. https://doi.org/10.1016/j.conbuildmat.2017.07.035

[17] S. Xu, H. Zhang, Y. Wang. Estimation of the properties of corroded steel plates exposed to salt-spray atmosphere [J]. Corrosion Engineering, Science and Technology, 2019, 54(5): 431-443. https://doi.org/10.1080/1478422X.2019.1613779

[18] H. Zhang, S. Xu, Z. Zhang, et al. Fracture analysis of corroded cold-formed thin steel plates based on actual morphology using micromechanical models [J]. Construction and Building Materials, 2021, 267: 120899. https://doi.org/10.1016/j.conbuildmat.2020.120899

[19] S.H. Xu, R. Gu, B. Nie, et al. Degradation law of mechanical properties of corroded cold-formed thin-walled steel sheet [J]. Journal of Harbin Institute of Technology, 2021, 53 (04): 177-186. (in Chinese)

[20] L. Chen, J.Z. Zhang, S.W. Liu, et al. Bifurcation buckling load of steel angle with corrosion damage [J]. Advanced Steel Construction, 2024, 20(2): 149-159. https://doi.org/10.18057/IJASC.2024.20.2.7

[21] K. Roy, H.H. Lau, Z. Fang, et al. Effects of corrosion on the strength of self-drilling screw connections in cold-formed steel structures-experiments and finite element modeling [C] //Structures. Elsevier, 2022, 36: 1080-1096. https://doi.org/10.1016/j.istruc.2021.12.052

[22] GB/T 10125-2021, Salt spray test for artificial atmosphere corrosion test [S]. Beijing: Standards Press of China, 2021. (in Chinese))

[23] GB/T 228.1-2021 Metallic materials-Tensile testing-Part 1: Method of test at room temperature [S]. Beijing: Standards Press of China, 2021. (in Chinese))

[24] J.R. Fu. Study on the mechanical properties of cold-formed thin-walled steel double-limb composite members with hybrid connection [D]. Southwest University of Science and Technology, 2023. (in Chinese)

[25] GB 50018-2002, Technical Code for Cold-Formed Thin-Walled Steel Structures [S]. Beijing: China Planning Press, 2002. (in Chinese)

[26] R.A. LaBoube, M.A. Sokol. Behavior of screw connections in residential construction[J]. Journal of structural engineering, 2002, 128(1): 115-118. https://doi.org/10.1061/(ASCE)0733-9445(2002)128:1(115)

[27] AISI S100-16, North American specification for the design of cold-formed steel structural members. Washington D C: American National Standards Institute, 2016.

[28] PREN1999-1-4, Eurocode 9: design of aluminium structures, part: 1-4: supplementary rules for cold-formed sheeting. Brussels: European Committee for Standardization (CEN), 2011.